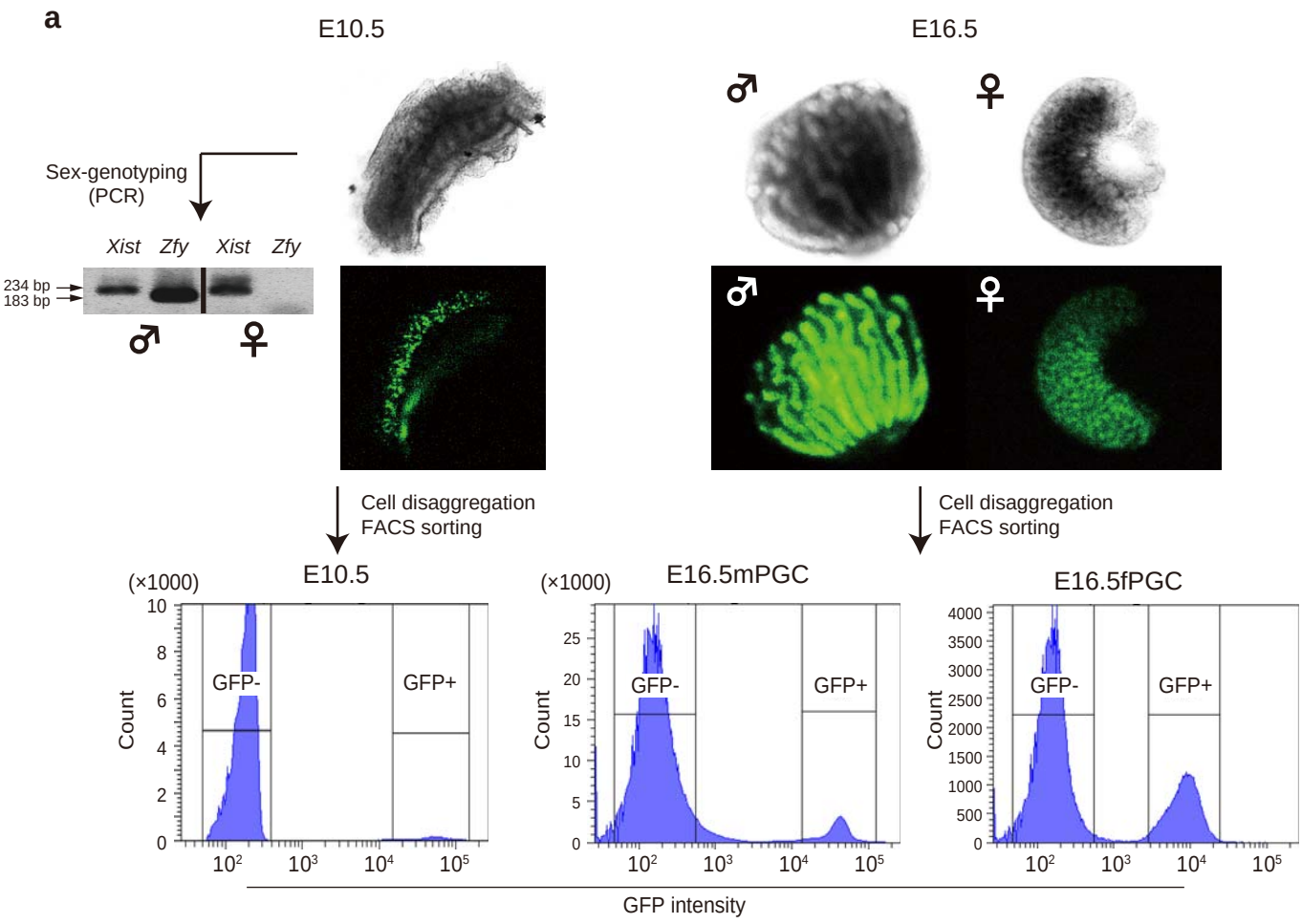

b

PGC counting by FACS

Developmental stage	PGCs/embryo
E10.5	200–300 cells
E13.5–E16.5	5,000–8,000 cells

Median values for GFP signals

Developmental stage	GFP intensity
E10.5–E13.5	30,000–50,000
E16.5 (male)	30,000–50,000
E16.5 (female)	10,000–15,000

c

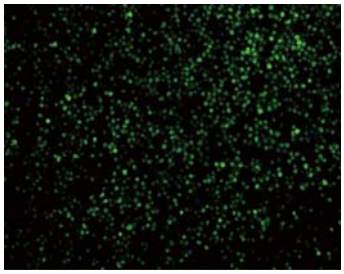

FACS-purified PGCs

Supplementary Figure 1

Isolation of mouse PGCs by FACS. (**a**) Schematic of PGC collection. Gonadal sexes were distinguished by PCR-based sex genotyping (E10.5) or morphology (E13.5 and E16.5). (**b**) PGC counts isolated from 1 embryo in each developmental stage by FACS. (**c**) FACS-purified PGCs observed under a fluorescence microscope (E13.5mPGC).

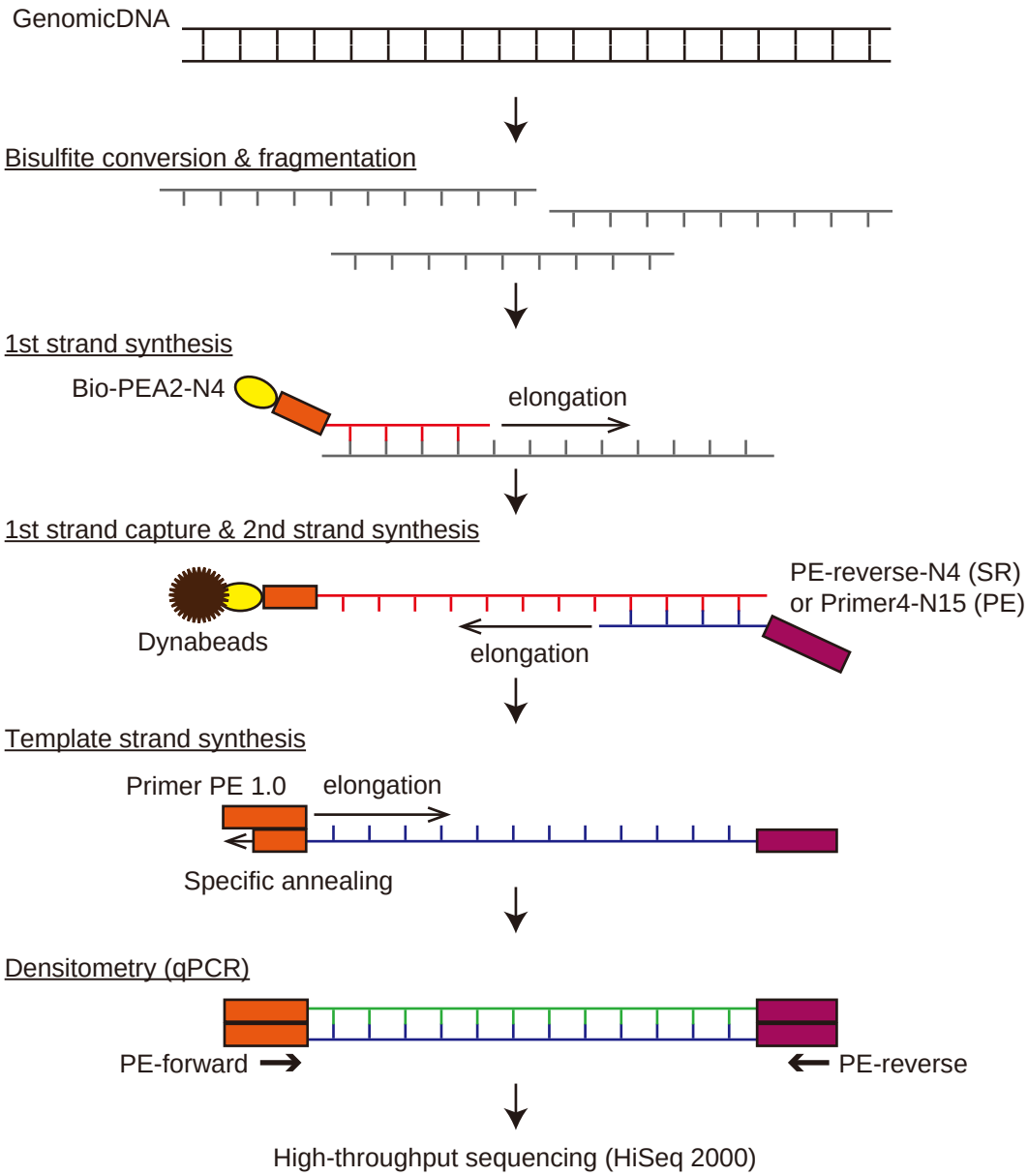

Supplementary Figure 2
Schematic of PBAT library preparation. PBAT is a new WGSBS method that accommodates low DNA input by preventing DNA damage due to bisulfite treatment (after adapter ligation, in the case of MethylC-Seq). Illumina adaptor-tagged WGSBS libraries were directly generated by 2 rounds of random priming on bisulfite-treated PGC genome DNA. The current protocol for PBAT uses a common primer named Bio-PEA2-N4 (for detailed sequence, see, Methods) for the first round of random priming. For second-round random priming, PE-reverse-N4 and Primer4-N15 are used for SE-read and PE-read sequencing, respectively. We noticed that the latter primer tends to bring fewer templates than the former primer, for unknown reasons (details will be published elsewhere). Readers should note the difference between the primers in the second-round reaction.

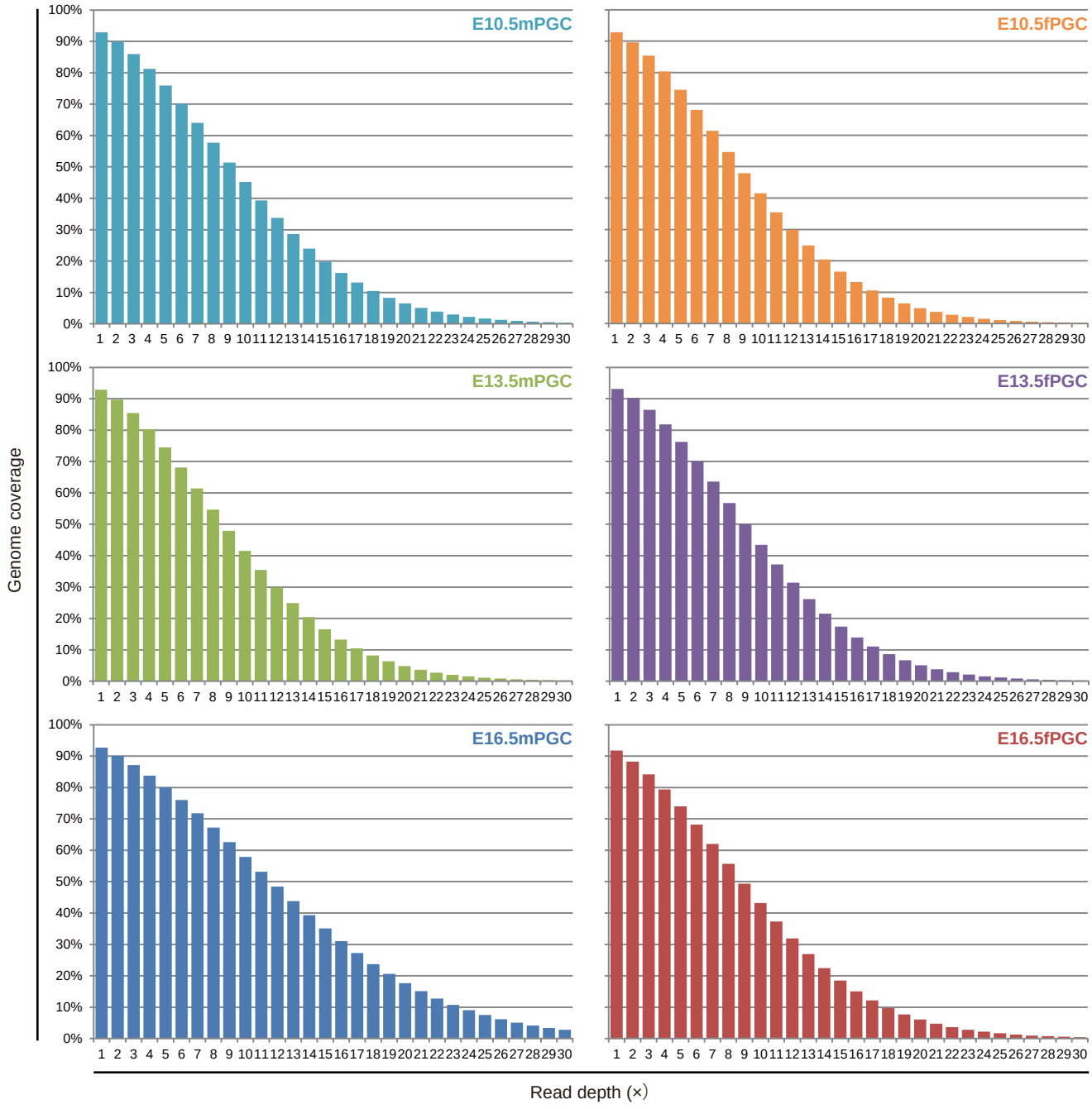

Supplementary Figure 3
Percentages of PGC genomes covered by differing minimum numbers (×1–30) of PBAT reads. E10.5mPGC, E10.5fPGC, E13.5mPGC, E13.5fPGC, E16.5mPGC, and E16.5fPGC are shown as aqua, orange, green, purple, blue, or red bars, respectively.

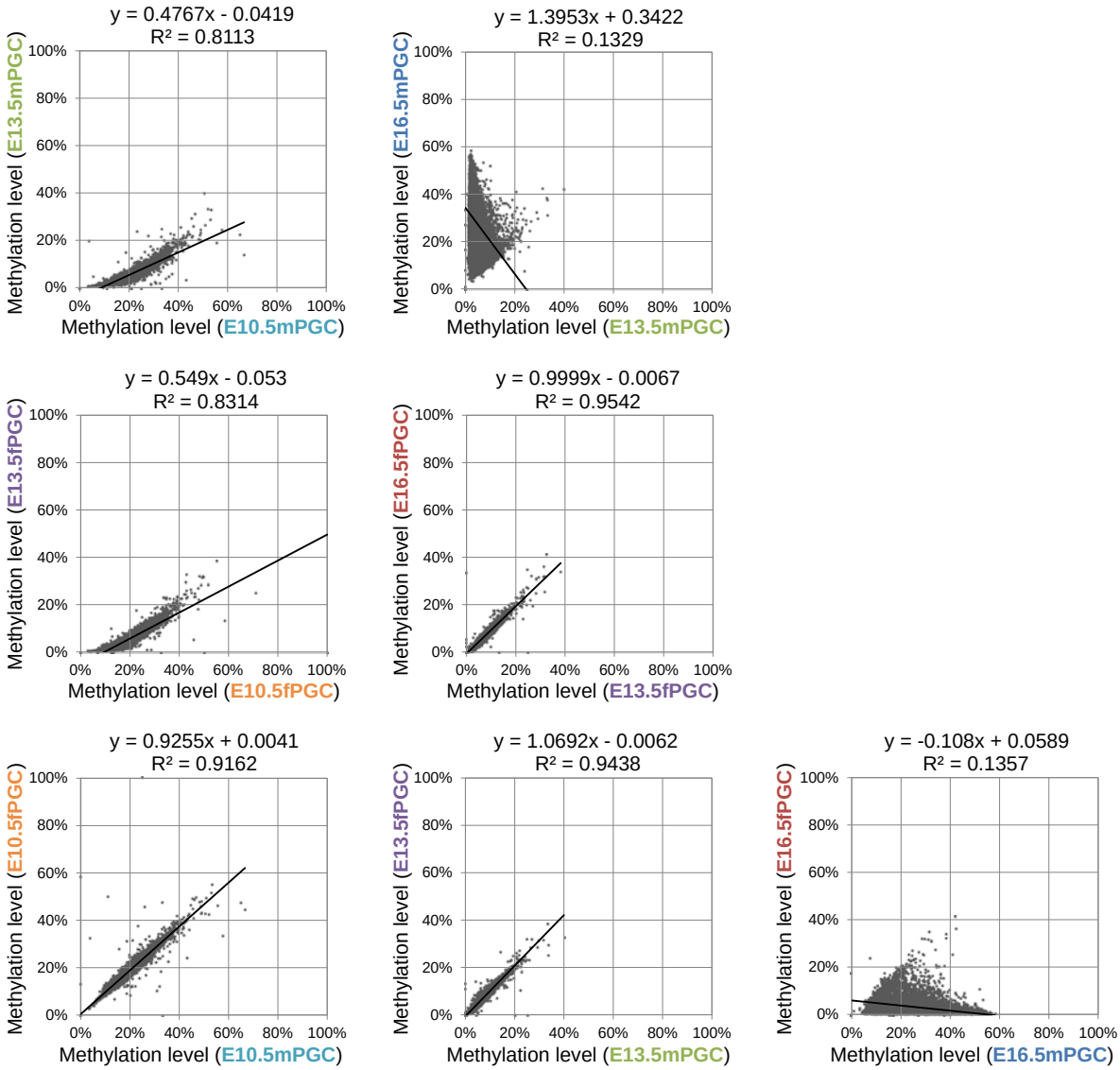

Supplementary Figure 4

Genome-wide correlation between CpG methylation profiles in sliding 200-kb windows. The scatter graphs show the relationships between the levels of regional DNA methylation (only chromosome Y was omitted) in male and female PGCs or developing (differential stage) PGCs. Linear approximations with squared correlation coefficient (R^2) values are shown at the top of each graph.

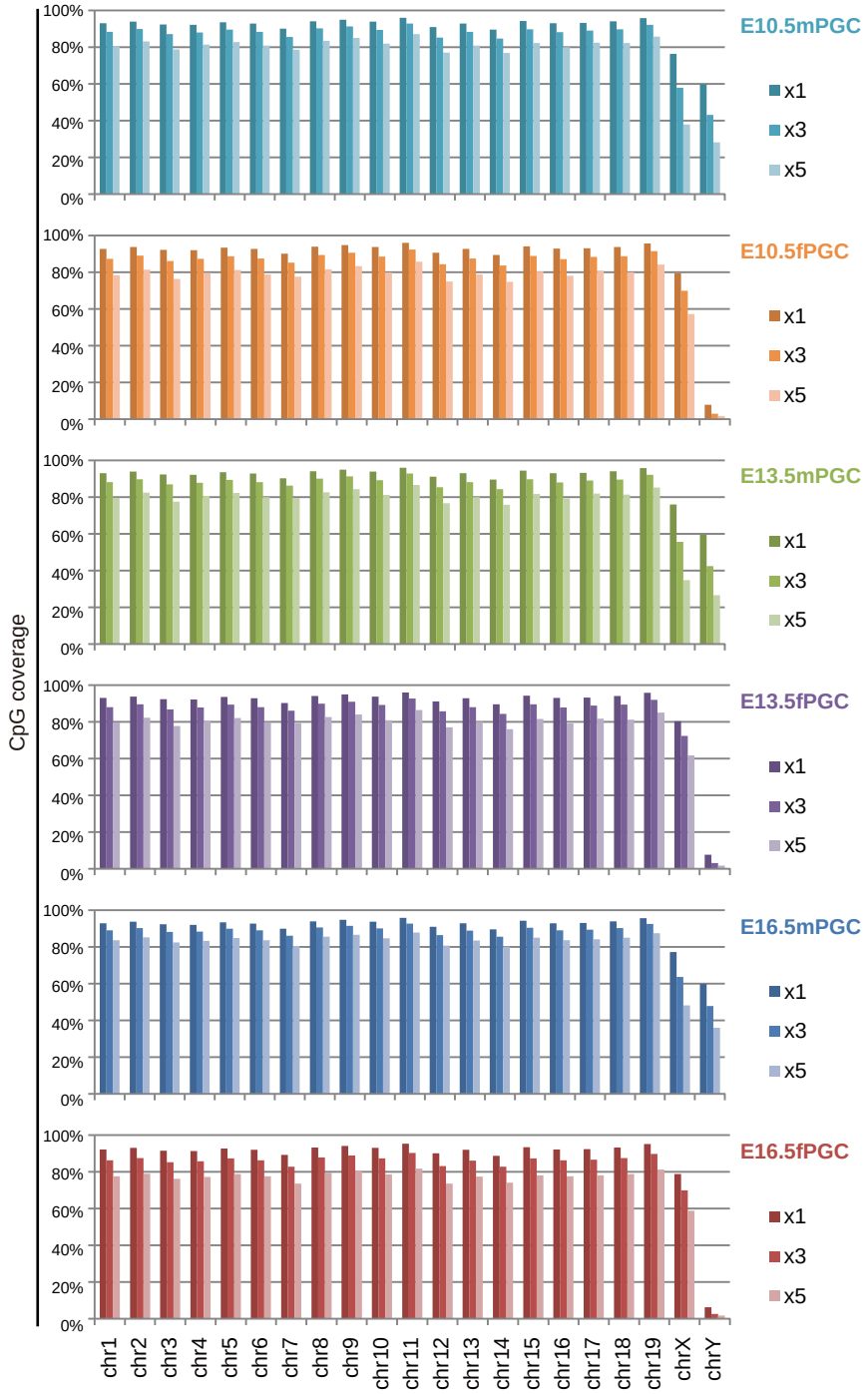

Supplementary Figure 5

Percentages of PGC genomic CpGs (on individual chromosomes) covered by differing minimum numbers (× 1, × 3, and × 5) of PBAT reads. Low coverage of the Y chromosome in female PGCs indicates that gender assignment of mesenteries/gonads was effectively managed by PCR-based sex genotyping or morphological analysis.

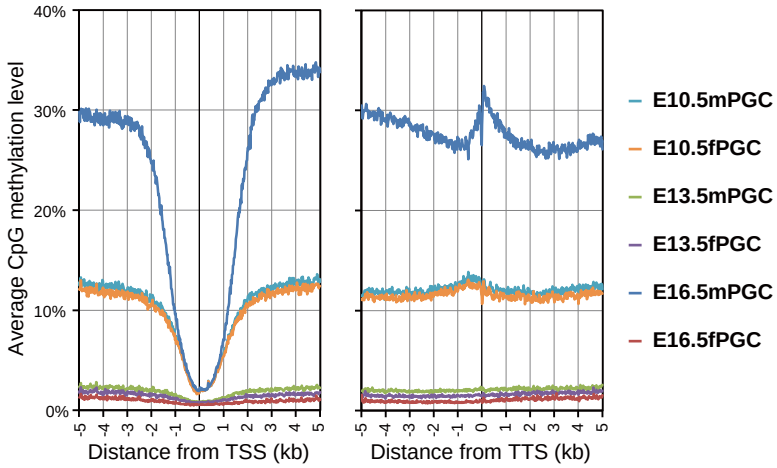

Supplementary Figure 6

The distribution of CpG methylation ± 5 kb from the transcription start site (TSS; *left*) and transcription termination site (TTS; *right*) in each PGC genome.

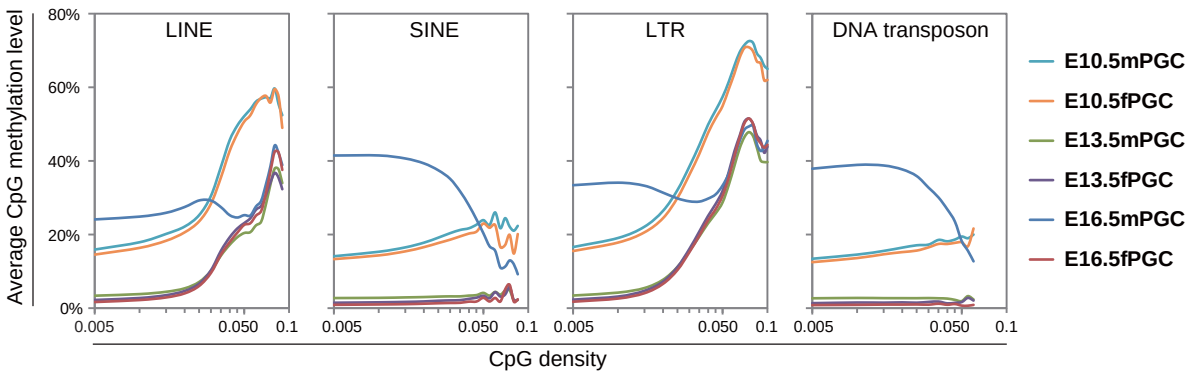

Supplementary Figure 7
DNA methylation profiling of TEs in mouse PGCs. CpG methylation levels are plotted as a function of CpG densities for 4 classes of TEs; LINEs, LTRs, SINEs, and DNA transposons.

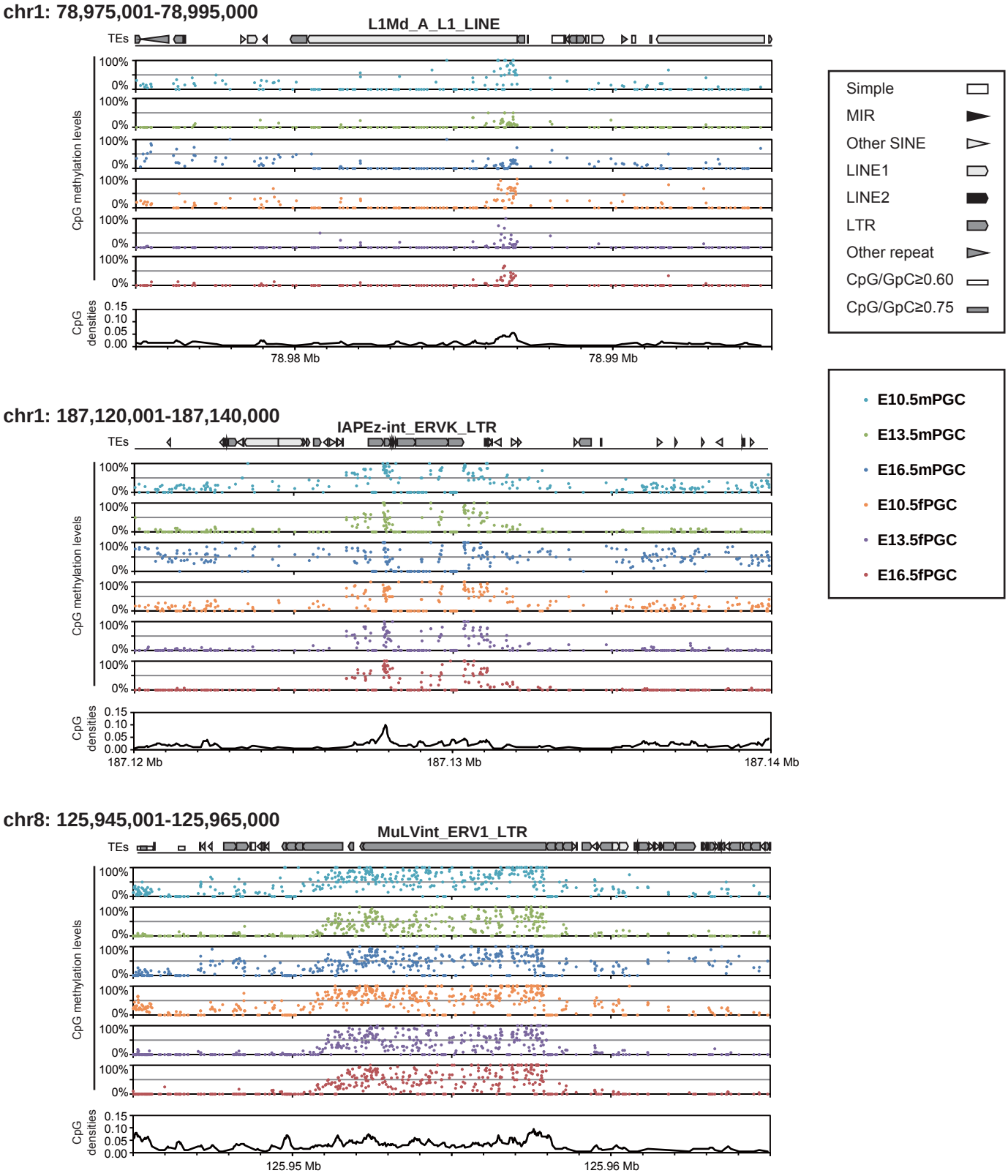

Supplementary Figure 8

DNA methylome maps of PGCs at 3 retrotransposon loci; L1 LINE, ERVK LTR (IAP), and ERV1 LTR, and their surrounding regions. Locations of TEs were shown at the top of graphs (plotted by PipMaker, http://pipmaker.bx.psu.edu/pipmaker/). The repeat files were generated by RepeatMasker (http://www.repeatmasker.org/). Aqua, green, blue, orange, purple, and red dots represent the methylation levels at individual CpGs in male PGCs at E10.5, E13.5, E16.5 and female PGCs at E10.5, E13.5, E16.5, respectively. Black line plots depict the distribution of CpG densities (number of CpG per 200 nt) of individual CpGs.

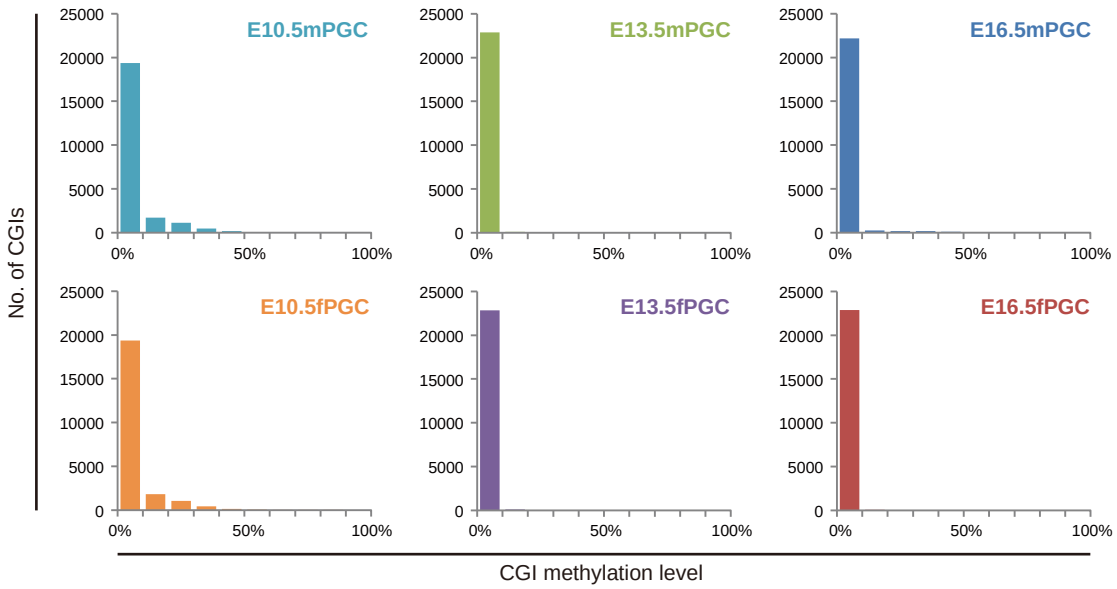

Supplementary Figure 9
Histograms of methylation levels of 23,021 CGIs in each PGC genome

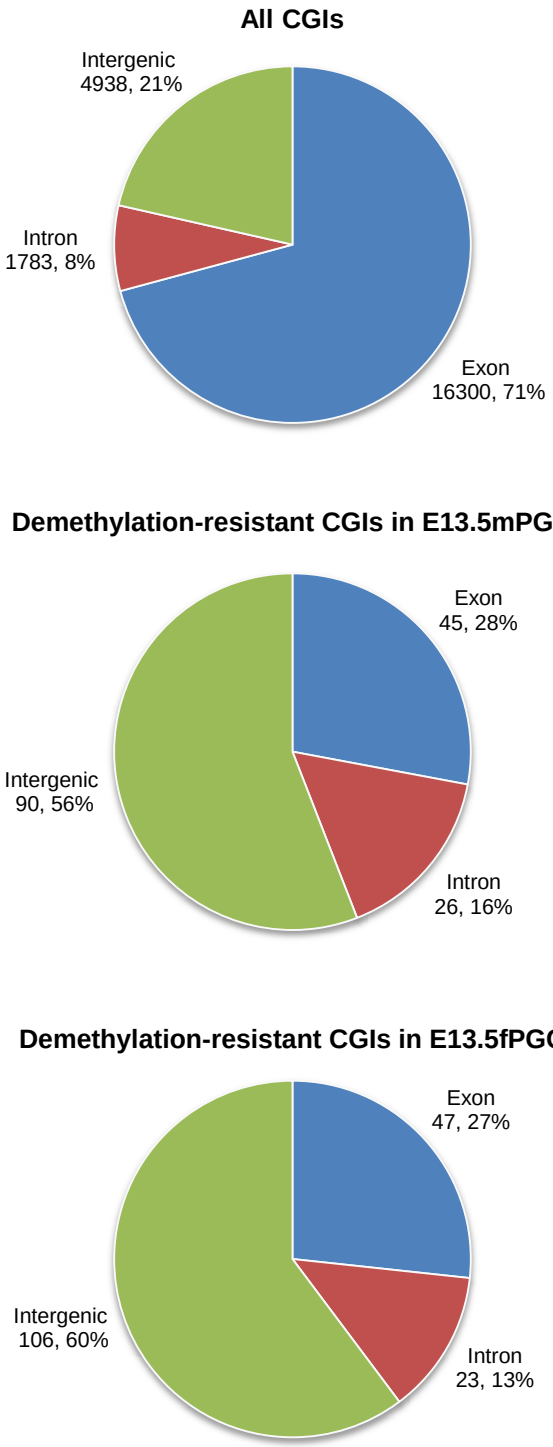

Supplementary Figure 10
Categorization of CGIs with respect to annotated genes (RefSeq) in mouse. Pie charts showing numbers and percentages of all (*top*) and demethylation-resistant (*middle*; in E13.5mPGC, *bottom*; in E13.5 fPGC) CGIs on exons, introns (intragenic regions excluding exons of any genes), and intergenic regions, respectively.

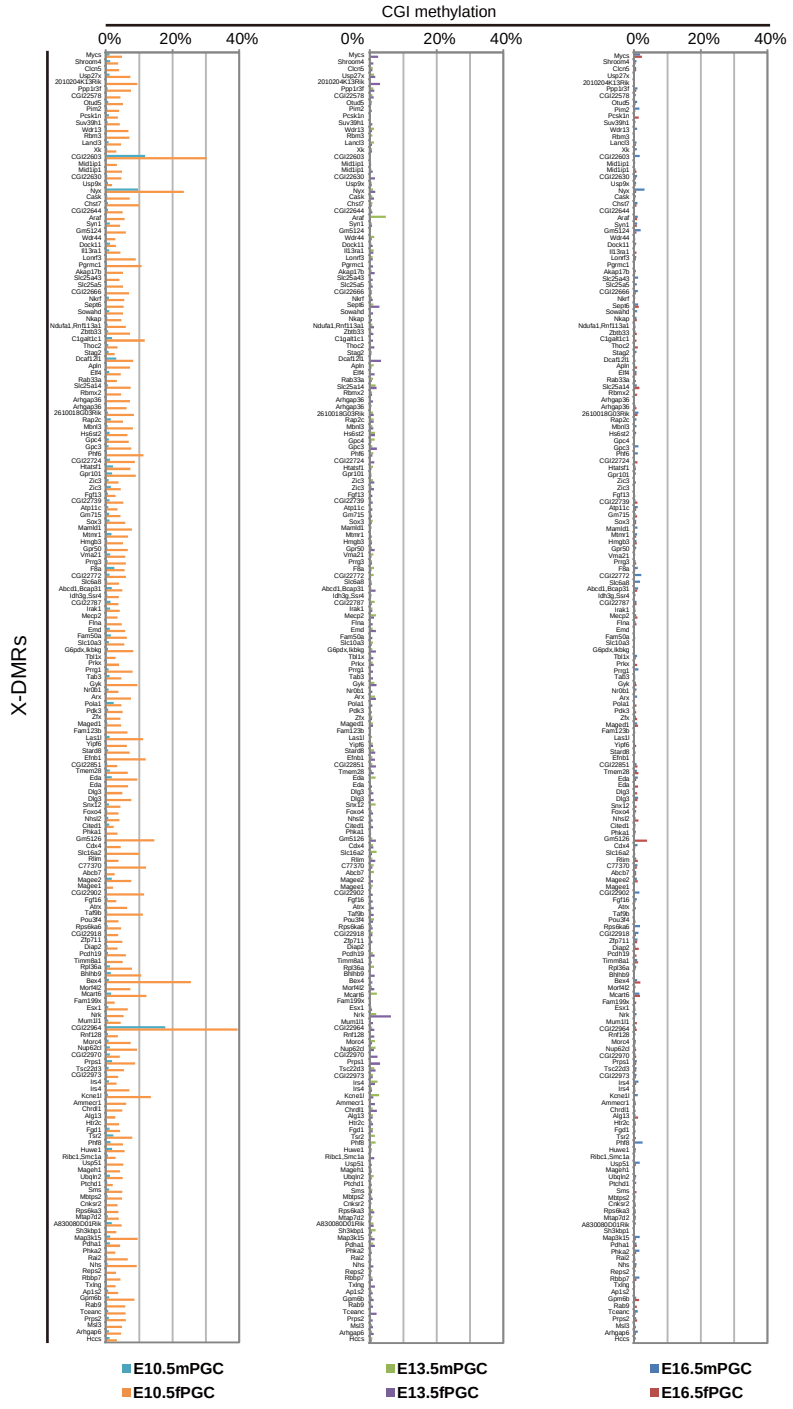

Supplementary Figure 11
Demethylation of X-DMRs after gonadal sex determination.

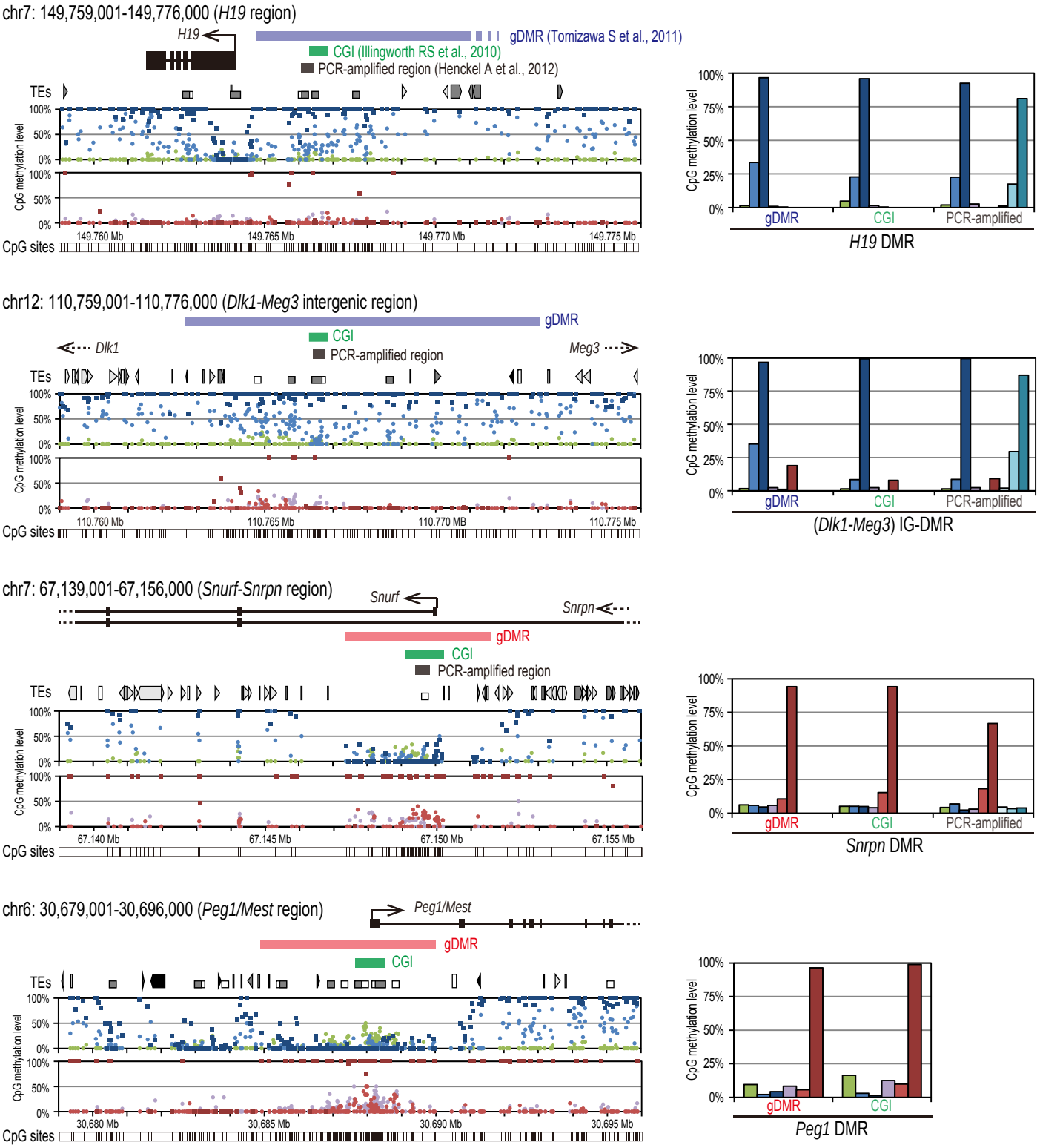

Supplementary Figure 12

DNA methylome maps (*left*) of PGCs (determined in this study) and fully-grown sperm and oocytes (determined by our previous data, Kobayashi et al. 2012) at 2 paternally methylated imprinted loci; *H19* and *Dlk1-Meg3* regions and 2 maternally methylated imprinted loci; *Snurf-Snrpn* and *Peg1*/*Mest* regions and CpG methylation profiling (*right*) at germline DMRs (gDMRs), their CGIs, and PCR-amplified regions reported by a previous conventional bisulfite sequencing study (Henckel et al. 2012) in individual imprinted loci. Extents of gDMRs (Tomizawa et al. 2011) and CGIs (Illingworth et al. 2010), and TE positions were shown at the top of graphs.

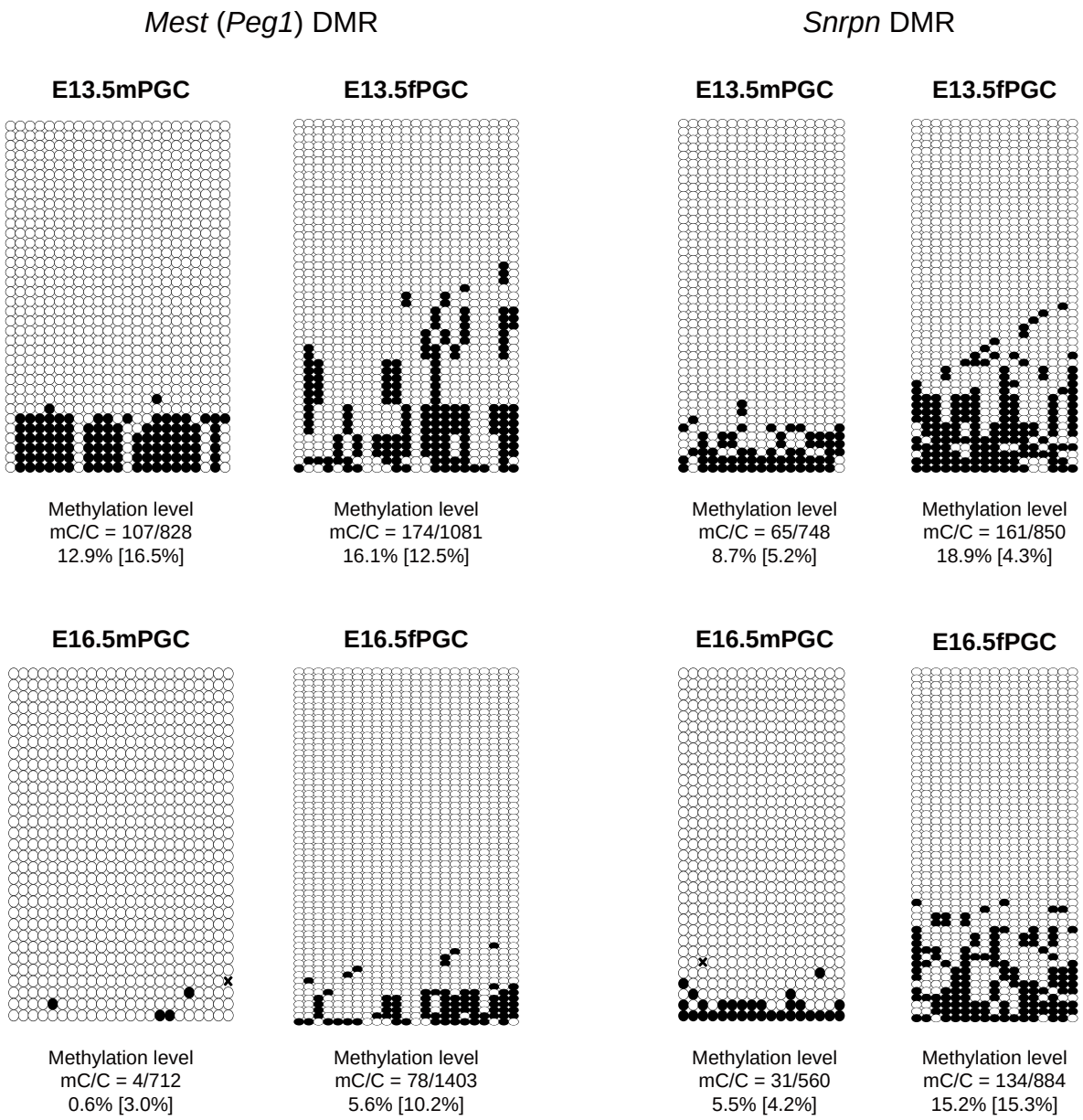

Supplementary Figure 13

DNA methylation profiles of Mest and Snrpn ICRs (DMRs) in male and female PGCs at E13.5 and E16.5 by conventional bisulfite sequencing. Each row of circles represents the results of an independent sequencing reaction. The open and closed circles denote unmethylated and methylated CpGs, respectively. Visualization and quantification of bisulfite sequence data for CpG methylation was performed using the QUMA web-based tool (http://quma.cdb.riken.jp/top/index.html). The calculated methylation levels are shown below the graphs. The methylation levels determined by WGSBS are given in brackets.

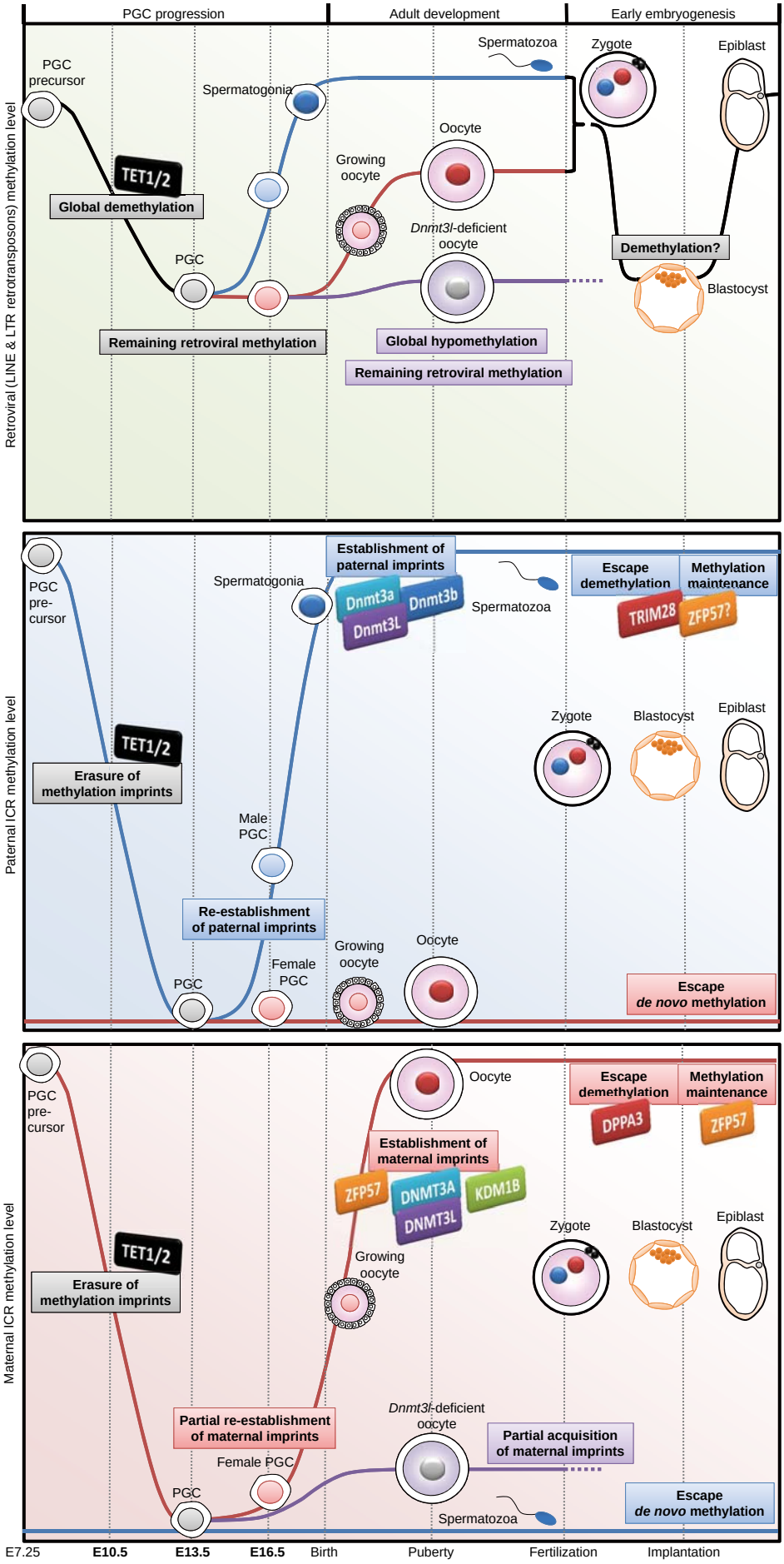

Supplementary Figure 14
Methylation dynamics of various sequence classes during mouse gametogenesis and embryogenesis.